nanomaterials

MDPI

Article

Interaction of Ethylene with Ir_n (n = 1–10): From Bare Clusters to γ-Al_2O_3-Supported Nanoparticles

Xue-Rong Shi [1,2,*], Yajing Zhang [1], Shibiao Zong [1], Wen Gu [1], Pan Ma [1] and Na Lu [1]

[1] School of Material Engineering, Shanghai University of Engineering Science, 333 Longteng Road, Songjiang District, Shanghai 201620, China; M050118113@sues.edu.cn (Y.Z.); M050117110@sues.edu.cn (S.Z.); guwen1-1@163.com (W.G.); mapan@sues.edu.cn (P.M.); 05160003@sues.edu.cn (N.L.)

[2] Institute of Physical Chemistry, University of Innsbruck, Innrain 80-82, Innsbruck A-6020, Austria

* Correspondence: shixuer05@mails.ucas.ac.cn; Tel.: +86-21-6779-1380

Received: 18 January 2019; Accepted: 20 February 2019; Published: 2 March 2019

Abstract: Comprehending the bond nature of ethylene-metal clusters at the atomic level is important for the design of nanocatalysts and their applications in the fields of fine chemistry and petroleum refining. The growth of Ir_n (n = 1–10) on γ–Al_2O_3(110) and ethylene adsorption on bare and γ–Al_2O_3(110)-supported Ir_n (n = 1–10) clusters were investigated using the density functional theory (DFT) approach. The mode stability of ethylene adsorption on the bare Ir_n clusters followed the order π > di-σ > B-T, with the exception of Ir_8 where the π structure was less stable than the di-σ configuration. On supported Ir_n (n = 4–7 and 10) the stability sequence was π > di-σ > di-σ' (at interface), while on supported Ir_n (n = 2, 3, 8, and 9) the sequence changed to di-σ > π > di-σ' (a interface). Two-thirds of ethylene adsorption on the supported Ir_n clusters were weaker than its adsorption on the bare Ir_n clusters. The pre-adsorbed ethylene at the interface was found to facilitate the nucleation from the even-sized supported Ir_n to odd-sized Ir_n clusters, but hindered the nucleation from the odd-sized Ir_n to even-sized Ir_n clusters.

Keywords: density functional theory (DFT); nucleation; metal clusters; alumina; ethylene

1. Introduction

Interaction of light alkenes with metal clusters has been widely studied in the past due to its important applications in the fields of fine chemistry and petroleum refining. As the smallest alkene and one of the most common probe molecules, the adsorption of ethylene on supported metal catalysts has been widely investigated [1–5]. Keppeler et al. [3] studied ethylene hydrogenation on the NaY and KL zeolite-supported Pt_{13} cluster and found ethane was the only product.

Recently, many experimental works [6–8] have investigated the properties of nanosized metal clusters on alumina support. D'Ippolito et al. [8] found that the addition of iridium to SiO_2–Al_2O_3 enhanced the decalin conversion in the selective ring opening reaction of decalin, while adding HCl barely affected the reaction. Argo et al. [9,10] found that iridium clusters (Ir_4 and Ir_6) on γ-Al_2O_3 rearranged slightly to adapt reactive intermediates in the reaction of ethylene hydrogenation, but remained intact using extended X-ray absorption fine structure (EXAFS) study.

Many efforts have been carried out to investigate the adsorption and nucleation of transition metals on alumina using first-principles calculations [11]. Wang et al. [12] studied the growth of Ir_n (n = 1–5) clusters on the dehydrated and hydrated γ-Al_2O_3 surfaces. They found the surface hydroxyl hindered the adsorption but facilitated the nucleation of Ir_n clusters. Chen et al. [13] investigated the nucleation of Ir_n (n = 2–10) clusters on dehydrated γ-Al_2O_3(001) and MgO(100) surfaces using density functional theory approach. They found that the growth of Ir_n (n = 2–10) on these two surfaces was

always exothermic. To our best knowledge, however, the study of ethylene interaction with bare Ir_n metal clusters and γ-Al_2O_3-supported Ir_n clusters is still unexplored.

The present work will focus on the effect of the support, which influences not only the adsorption performance of ethylene on Ir_n, but also the structural features and cluster stability of the nanosized iridium. For this purpose, we use the DFT calculations to explore the growth of Ir_n (n = 1–10) clusters on γ-Al_2O_3 and discuss the interaction of ethylene with the bare and γ-Al_2O_3-supported Ir_n (n = 1–10) clusters. According to the previous work [14–17], the γ-Al_2O_3 surface probably is covered by the hydroxyl groups and the corresponding coverage of surface hydroxyl depends on the preparation temperature. In the reaction of ethylene hydrogenation, the γ-alumina-supported Ir catalysts are typically calcined at 598–673 K during the pretreatment process [9,10]. To correctly describe the surface structures under experimentally relevant conditions, we employ the surface structure constructed by Digne et al. [16] to perform our studies.

2. Materials and Methods

The hydrated γ-Al_2O_3(110) surface with a hydroxyl coverage of 5.9 OH/nm^2 at 673 K was constructed according to [16]. As shown in Figure 1, the covering hydroxyl groups and the surface Al and O atoms on this hydrated (110) surface formed a distinct valley. To prevent the interaction between the neighboring Ir_n clusters, a large slab of 2 × 2 unit cell (surface area is ~272 Å^2) with four layers of thickness containing 224 atoms was employed. Only the bottom two layers were fixed during the geometry optimizations. For the bare Ir_n systems, all atoms were relaxed.

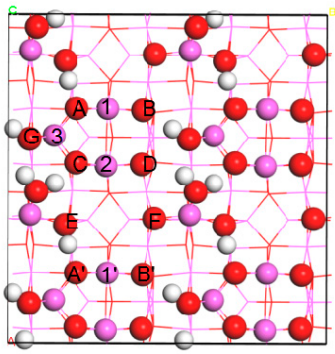

Figure 1. Top view of hydrated γ-Al_2O_3(110) surface with 5.9 OH/nm^2. Atoms in the first layer and other layers are displayed in sphere and line forms, respectively. White: H, red: O, and pink: Al.

We used the the Vienna ab initio simulation package (VASP) [18,19] to perform the spin-polarized DFT calculations. The Perdew–Wang exchange-correlation functional [20,21] and projector augmented wave (PAW) method [22] were employed with a cutoff energy of 400 eV. The force threshold of geometry optimization was set to 0.03 eV/Å. A gamma K-point for optimizations and 4 × 4 × 1 K-points for electronic structure calculations were used. All parameters in our calculations were carefully tested, with the change of the calculated E_{ads} smaller than 2%.

The adsorption energy E_{ads} of adsorbates species on substrate was calculated using

$$E_{ads} = E(Ads/Sub) - E(Sub) - E(Ads) \quad (1)$$

E(Ads/Sub), E(Sub), and E(Ads) are the total energies of the energy minimized substrate with adsorbates, bare substrate, and gas-phase adsorbates, respectively.

The deformation energy of the adsorbate between its equilibrium structure in the gas phase and the adsorbed state was calculated by

$$E_{def}(Ads) = E(Ads') - E(Ads) \quad (2)$$

Here E(Ads′) is the total energy of adsorbate species in the gas phase employing the structure displayed in the adsorbed state. Similarly, the deformation energy of the substrate E_{def}(Sub) was calculated by

$$E_{def}(Sub) = E(Sub') - E(Sub) \quad (3)$$

E(Sub′) is the total energy of the substrate retaining the adsorbed geometry, but with the adsorbates removed. The adsorbate–substrate interaction energy E_{int} was calculated by

$$E_{int} = E(Ads/Sub) - E(Ads') - E(Sub') \quad (4)$$

For ethylene adsorption, the corresponding adsorption Gibbs free energy ΔG_{ads}(T, P) was defined using

$$\Delta G_{ads}(T, P) = E_{ads} - G^{\Theta}(T) - RTln(P_{C2H4}/P^{\Theta}) \quad (5)$$

G^{Θ}(T) contains the thermodynamical items of translation, vibration, and rotation of ethylene molecules in the gas phase. P_{C2H4} is the partial pressure of ethylene. We include zero-point vibrational energy in our present work. A detailed description of Equation (5) can be found in our previous work [23].

3. Results and Discussion

3.1. Gas-Phase Clusters

The structures of gas-phase Ir_n (n = 2–10) clusters, which are critical to comprehending the nucleation of Ir_n clusters on γ-Al_2O_3, have been well studied before [12,13]. Thus, although we considered different gas-phase Ir_n structures, only the most favorable geometries with the lowest energy are summarized in Table S1. The energetically preferred geometries for Ir_n (n = 3–8) were linear ($D_{\infty h}$), square planar (in D_{4h}), square pyramid (C_{4v}), triangular prism (D_{3h}), side-face-capped triangular prism (C_{2v}), and cubic structure (O_h), respectively. The Ir_9 cluster presented a C_s point group with one Ir atom bridged on two neighboring edge Ir atoms of the cube. The most stable Ir_{10} geometry yielded the configuration with the Ir_2 dimer capping on one face of the cube. The Ir–Ir distance of the Ir_n (n = 2–10) clusters was in the range of 2.18–2.51 Å, which was shorter than the bulk Ir–Ir distance of 2.74 Å. A similar bond contraction was observed for the bare Rh clusters without ligands experimentally [24] and theoretically [25].

3.2. Small Ir_n Clusters on Hydrated γ-Al_2O_3(110)

For Ir adsorption, we considered a series of adsorption sites including seven top (O(A), O(B), O(C), O(D), O(F), Al(1), and Al(2)), ten bridge (O(A)-O(C), O(B)-O(D), O(D)-O(F), O(B′)-O(F), Al(1)-Al(2), Al(1′)-Al(2), O(A)-Al(1), O(B)-Al(1), O(C)-Al(2), and O(D)-Al(2)), and three hollow sites (O(A)-O(C)-Al(3), O(D)-O(F)-Al(2), and O(B′)-O(E′)-O(F)) (Figure 1). The most energetically favorable structures and corresponding adsorption energies E_{ads} are summarized in Figure 2 and Table S2, respectively.

As shown in Figure 2, a single Ir atom preferred to bond to surface Al(1), Al(2), and O(A) atoms yielding E_{ads} of −2.58 eV. For Ir_2 adsorption, both Ir atoms bonded to the surface, forming three Ir–Al bonds and two Ir–O bonds with E_{ads} of −2.53 eV. Two Ir atoms bonded to the same surface Al center.

Unlike the case in the gas phase, the adsorbed Ir_3 preferred the triangular configuration over the linear one. The adsorbed triangular structure presented E_{ads} of −3.67 eV with respect to the gas-phase triangular trimer, which was 1.14 eV lower in energy than the linear structure, while in the gas phase the former was 0.26 eV higher than the latter. The adsorbed triangular trimer presented a stand-up configuration with two Ir atoms binding to the surface and one Ir atom pointing to the air. While in the adsorbed linear trimer, each Ir atom bonded to the surface.

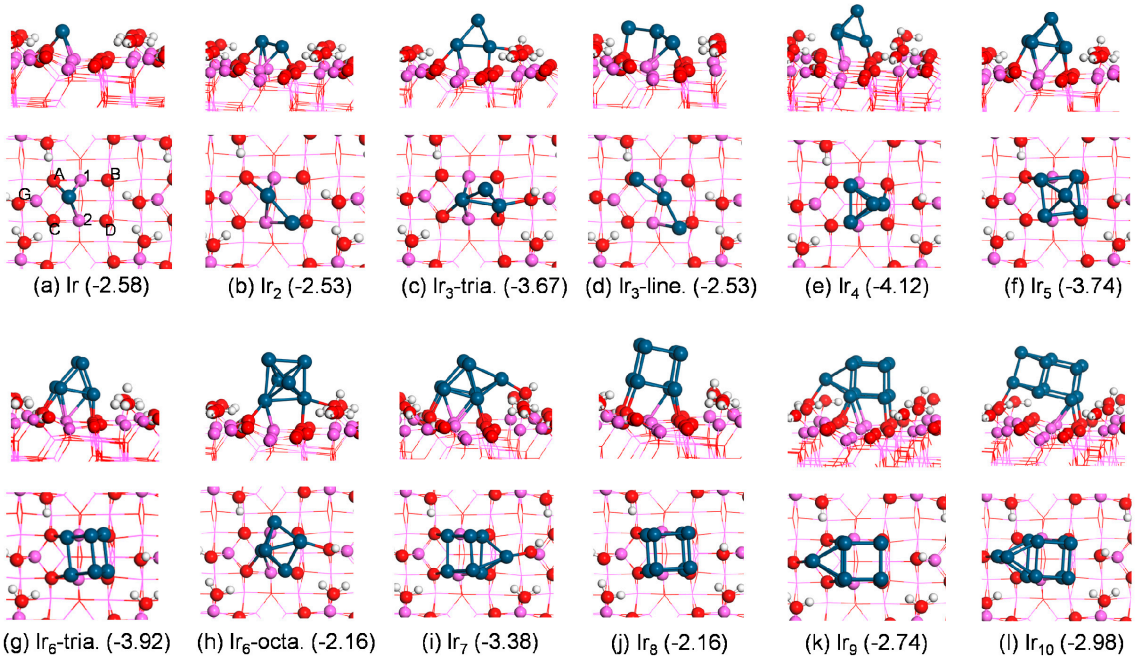

Figure 2. Side (top) and top views (bottom) of the most favorable Ir_n (n = 1–10) adsorption structures with the corresponding adsorption energies E_{ads} (in eV) on the hydrated γ-Al_2O_3(110) surface. Largest spheres: Ir; the other color/label scheme is identical to Figure 1.

For Ir_4 adsorption, all attempts to obtain the square planar Ir_4 cluster (the most stable configuration in gas phase) converted to the geometry with a bent rhombus on the surface. The reconstruction of small deposited metal clusters on the support was also observed for Pd_n clusters (n = 1–7) adsorption on α–Al_2O_3 (0001). Nigam and Majumder [26] found that the Pd_4 deformed from the tetrahedral configuration in the gas phase into the bent rhombus in the adsorbed state on the Al_2O_3 surface. The most stable structure was a tetrahedron with three Ir atoms bonding to the surface and resulting in E_{ads} of −4.12 eV. Our results agree with the earlier experimental and theoretical reports. Using EXAFS spectroscopy, Argo et al. [9] found an Ir–Ir first-shell coordination number in γ-Al_2O_3-supported Ir_4 nanoparticles of about 3. Our previous study showed that Rh_4 also prefers the tetrahedral frame on γ-Al_2O_3 surfaces [25].

The adsorbed Ir_5 retained the square pyramid geometry upon adsorption on the surface, with four Ir atoms bonding to the substrate and yielding E_{ads} of −3.74 eV.

Analogous to the case in the gas phase, the most energetically preferred Ir_6 geometry was a triangular prism with E_{ads} of −3.92 eV. In the adsorbed state, four Ir atoms made contact with the substrate and two Ir atoms kept away from the surface. The most stable octahedral structure of adsorbed Ir_6 was less stable by 1.76 eV (higher in energy) than the triangular prism on the γ-Al_2O_3 support, and in the gas phase the energy difference between each was 0.70 eV. The coordinates RMSD (root-mean-square deviation) between the triangular prism configuration and the octahedral structure for the Ir_6 cluster were ~0.94 in the gas phase and ~0.98 for the supported case, respectively, which is consistent with the energy difference between the two. The octahedral adsorbed Ir_6 cluster bonded to the substrate via two Ir atoms (Figure 2h). This was inconsistent with the experimental observation [9,26,27], but in agreement with the previous calculations [13,28,29]. Experimentally, the octahedral Ir_6 commonly exists in the form of Ir_6 complexes [9]. Argo et al. [9] used the octahedral frame of $[Ir_6(CO)_{15}]^{2-}$ upon its decarbonylation to obtain an Ir_6 cluster on the γ-Al_2O_3 support and found that Ir_6 maintained the octahedral frame after decarbonylation using EXAFS measurements. Here, the CO ligands helped it to keep the octahedral frame, while several theoretical studies [13,28,29] found that the bare gas-phase Ir_6 cluster without any ligand favored a triangular prism with D_{3h} symmetry over the O_h octahedral structure.

For Ir_7 adsorption, the energetically preferred structure yielded a similar configuration to the gas-phase cluster with E_{ads} of −3.38 eV. The additional Ir atom to the adsorbed triangular prism Ir_6 cluster bonded to the oxygen atom in a surface hydroxyl. A surface distortion (Figure 2i) was observed upon the adsorption of the Ir_7 cluster, where the bonded hydroxyl moved upwards to make contact with the Ir atom. The similar adsorbate-induced support rearrangement was found for triangular Ir_3 adsorption on γ-Al_2O_3 (Figure 2c).

The most stable configuration for Ir_8 adsorption on alumina was a cubic Ir_8 cluster with four Ir atoms bonding to the surface and resulting in E_{ads} of −2.16 eV (Figure 2j). The most favorable structures for Ir_9 and Ir_{10} adsorption exhibited E_{ads} of −2.74 and −2.98 eV, respectively. As shown in Figure 2k,l, one Ir atom in the adsorbed Ir_9 and Ir_{10} cluster bonded to the oxygen center in a surface hydroxyl group.

Similar to our previous finding for Rh adsorption on the hydrated γ-Al_2O_3(110) surface [25], Ir_n clusters preferred to adsorb in the valley of the surface O and Al sites instead of on the covering hydroxyls layer, indicating the nanosized metal cluster can retard the transformation of γ-Al_2O_3 to AlOOH by pre-adsorption on the transformation site. This is consistent with the previous experimental [30] and theoretical [25] observations, confirming that it may be a general effect for a large number of nanosized transition metals.

In summary, Ir_n preferred to adsorb on the no-hydroxyls-covered area. When cluster diameter (to simplify, the cluster diameter is defined by the longest distance of M–M in the cluster) was smaller than 4.11 Å (e.g., n = 1–6 and 8), the Ir_n cluster bonded to the surface O and Al atoms only. When cluster diameter was larger than 4.21 Å (n = 7, 9, and 10), besides bonding to the surface O and Al atoms, the Ir_n cluster bonded to the oxygen of surface hydroxyl as well. The γ–Al_2O_3 (110) support changed the morphological features and the cluster stability of Ir_3 and Ir_4 upon their adsorption on the support. The Ir–Ir distance of adsorbed Ir_n (n = 2–10) in the basal plane underwent an elongation compared with the gas-phase Ir_n clusters.

3.3. Adsorption of Ethylene on Bare Ir_n

For ethylene adsorption on the bare Ir_n cluster, three adsorption modes were considered: di-σ mode, with two carbon ends of ethylene binding to two substrate atoms; π mode, with two carbon ends of ethylene binding to one substrate atom; and a bridge-top (B-T) mode, with one carbon bridging two substrate atoms and the other carbon binding to one substrate atom.

Ethylene adsorption on atomic Ir yielded the largest E_{ads} of −2.96 eV, suggesting the strongest ethylene binding of all considered Ir_n (n = 1–10) clusters (Table 1). Ethylene adsorption on the Ir_2 cluster (Figure 3a) via π-bound mode yielded an adsorption energy E_{ads} of −1.79 eV, which was very close to the di-σ-bound mode that featured E_{ads} of −1.75 eV. This suggests very similar adsorbate binding for both modes at 0 K.

Geometry optimization of ethylene adsorption on the bare Ir_3 cluster yielded three different local-energy minima, and those with the lowest total energy for each mode are shown in Figure 3b. The E_{ads}, −1.82 eV (π-bound mode) and −1.75 eV (di-σ-bound mode), differ only slightly. The adsorption of ethylene induced a strong deformation of the Ir_3 cluster, where Ir_3 changed from the linear structure in the free phase to the bent configuration with the adsorbate. The deformation energy $E_{def}(Ir_3)$ reached as high as 0.23 (0.15) eV for the π (di-σ)-bound mode.

For ethylene adsorption on the square Ir_4 cluster (Figure 3c), the calculations found two local equilibrium geometries for each mode. The π-bound state was more favorable than the di-σ-bound mode, where E_{ads} of the π-bound mode was −2.46 eV and the di-σ-bound state yielded E_{ads} of −1.89 eV. To compare with the supported Ir_4 cluster, ethylene adsorption on the bent-rhombus Ir_4 cluster was studied as well. Ethylene adsorption yielded four di-σ and two π local minima, and the energetically preferred structure for each mode is provided in Figure 3d. The di-σ mode was less stable than the π mode by 0.24 eV (higher in energy).

Ethylene adsorption on Ir_5 (two local equilibrium geometries for each mode are found) preferred the π-bound state to the di-σ-bound mode, which accounts for E_{ads} of −2.30 eV (π) and −1.80 eV (di-σ).

Ethylene stabilizes on the triangular-prism Ir_6 cluster, and the most favorable adsorption geometries are shown in Figure 3f. Ethylene adsorption on the triangular-prism Ir_6 preferred the π state to the di-σ mode. The corresponding adsorption energies were −2.06 and −1.84 eV for the π-bound state and di-σ-bound mode, respectively. Similarly, ethylene adsorption on the octahedral Ir_6 cluster (Figure 3g) via the π-bound state was more stable than it was via the di-σ-bound mode, with an energy difference of 0.46 eV.

Geometry optimization of ethylene adsorption on the Ir_7 cluster yielded three π and four di-σ local-energy minima. The most stable adsorption geometries of ethylene on the Ir_7 cluster for each mode are sketched in Figure 3h. Our results show that the π structure yields E_{ads} of −1.94 eV, which is more favorable than the di-σ structure by 0.09 eV (lower in energy).

The energetically preferred adsorption geometries of ethylene on the Ir_8 cluster are sketched in Figure 3i. The calculations yield E_{ads} of −1.63 eV (π) and −1.76 eV (di-σ), suggesting stronger binding for the di-σ structure compared with the π state.

For ethylene adsorption on Ir_9, the calculations found three π and five di-σ local-energy minima structures, and the most stable one is shown in Figure 3j. The most stable π and di-σ structures yielded E_{ads} of −2.11 and −1.82 eV, respectively, indicating a stronger stability of the π mode.

The most stable adsorption geometry of ethylene on the bare Ir_{10} cluster via π-bound mode (of three local equilibrium geometries found) is sketched in Figure 3k. The stability of ethylene adsorption decreased in the sequence of π > di-σ > B-T. Among the obtained three local equilibrium geometries, the most stable π structure yielded E_{ads} of −1.88 eV, which was 0.11 eV lower than the most stable di-σ structure (of seven local equilibrium geometries). Two di-σ structures yielded identical E_{ads} of −1.77 eV. The B-T configuration (Figure 3k) was the least stable, with much smaller E_{ads} of −0.02 eV. Note that the B-T structure was only available on Ir_{10}. All attempts to obtain the B-T configuration on the other Ir_n clusters resulted in either the π structure or the di-σ mode.

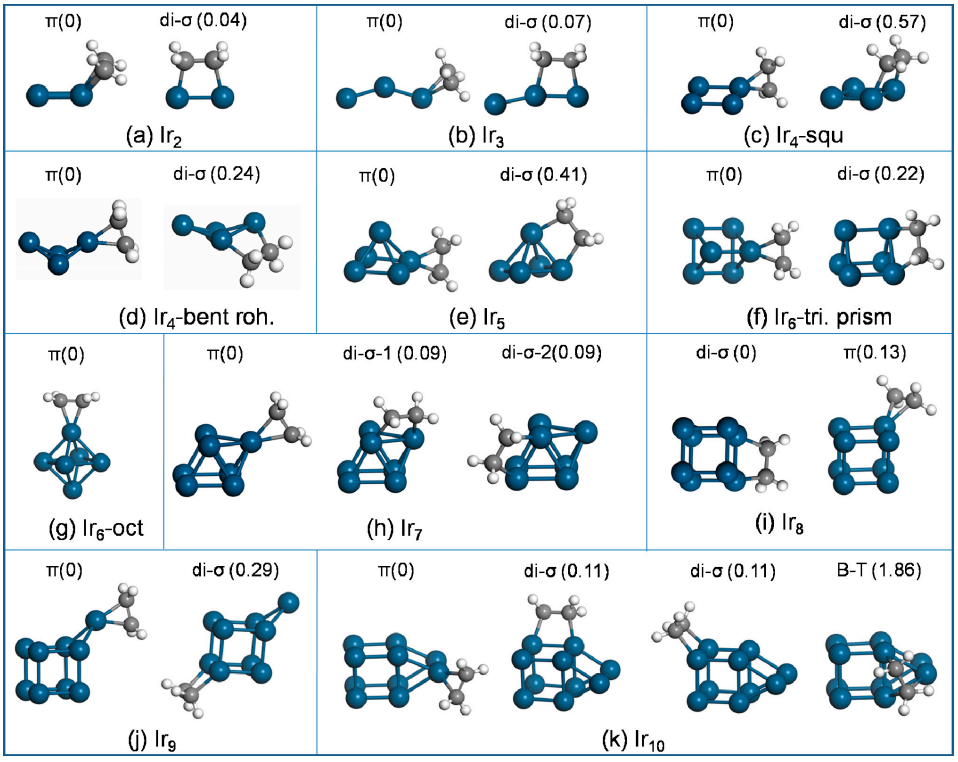

Figure 3. The most stable structure for each ethylene-binding mode on bare Ir_n. The energy difference (eV) with respect to the most stable configuration (energy set to 0) is labeled at the top of the figure.

In summary, the stability of ethylene adsorption on the bare Ir_n clusters decreased in the sequence of π > di-σ > B-T with one exception of Ir_8 where the di-σ structure was energetically preferred over the π structure.

To analyze the adsorption energy in more details, we divided it into three contributions according to $E_{ads} = E_{def}(C_2H_4) + E_{def}(Ir_n) + E_{int}$. From the data summarized in Table 1, we can see that the ethylene deformation energies for the di-σ and π structures were within the energy range of 1.53–1.85 and 0.45–0.53 eV, respectively. The deformation energy of ethylene accompanied the adsorption of ethylene along with the C−C bond elongation. The di-σ structure always induced a greater elongation regarding the gas phase than the π mode in our studies, which is in agreement with previous theoretical studies [31,32]. The C−C bond distance in the di-σ mode enlarged to ~1.51Å from 1.33 Å in the gas phase, while the π mode caused a smaller C−C bond extension (~1.43 Å).

Further analysis shows that the deformation of the adsorbate was much stronger than that of the substrate. As the deformation energies of the adsorbed ethylene were larger than 0.45 eV, the deformation energies of Ir_n clusters were rather small, below 0.23 eV. The energy cost for the deformation could have been compensated by the interaction energy between the adsorbates and the substrate. Despite the cluster–ethylene interaction energy in the di-σ mode always being larger than that in the π mode, it could not compensate for the energy cost difference of the deformation between two modes on most of the Ir_n clusters (excluding Ir_8). As a result, ethylene preferred to adsorb on the bare clusters via the π mode, except for the Ir_8 cluster. The reverse preference of adsorption mode on Ir_8 was the same with Ir(111) [33], where the di-σ mode was more favorable than the π mode.

Table 1. Adsorption energy E_{ads} (eV), standard adsorption Gibbs free energy at 300 K with the partial pressure of ethylene at 1atm $\Delta G^{\ominus}_{ads}$(300 K) (eV), ethylene deformation energy $E_{def}(C_2H_4)$ (eV), Ir_n cluster deformation energy $E_{def}(Ir_n)$ (eV), interaction energy E_{int} (eV), carbon–carbon bond distance $d_{C\text{-}C}$ (Å), and mean hybridization value (hyd.) for ethylene adsorption on bare Ir_n (n = 1–10) clusters.

n	mode	E_{ads}	$\Delta G^{\ominus}_{ads}$(300 K)	$E_{def}(C_2H_4)$	$E_{def}(Ir_n)$	E_{int}	$d_{C\text{-}C}$	hyb.
1	π	−2.96	−3.70	0.63	0	−3.59	1.44	2.50
2	π	−1.79	−2.53	0.52	0.02	−2.33	1.44	2.44
	di-σ	−1.75	−2.49	1.85	0.15	−3.75	1.53	2.89
3	π	−1.82	−2.56	0.52	0.23	−2.57	1.43	2.45
	di-σ	−1.75	−2.49	1.53	0.15	−3.43	1.51	2.84
4squ	π	−2.46	−3.20	0.48	0.02	−2.96	1.43	2.42
	di-σ	−1.89	−2.63	1.70	0.11	−3.70	1.52	2.84
4ben	π	−2.25	−2.99	0.50	0.12	−2.87	1.43	2.42
	di-σ	−2.01	−2.75	1.60	0.11	−3.72	1.51	2.84
5	π	−2.30	−3.04	0.52	0.02	−2.84	1.43	2.44
	di-σ	−1.89	−2.63	1.71	0.04	−3.64	1.51	2.89
6tri	π	−2.06	−2.80	0.55	0.04	−2.65	1.44	2.45
	di-σ	−1.84	−2.58	1.65	0.01	−3.50	1.51	2.84
6oct	π	−2.02	−2.76	0.57	0.06	−2.65	1.44	2.47
	di-σ	−1.56	−2.30	1.75	0.14	−3.45	1.52	2.86
7	π	−1.94	−2.68	0.54	0.01	−2.49	1.44	2.42
	di-σ	−1.85	−2.59	1.68	0.17	−3.70	1.51	2.86
8	π	−1.63	−2.37	0.54	0.17	−2.34	1.44	2.46
	di-σ	−1.76	−2.50	1.74	0.08	−3.58	1.52	2.84
9	π	−2.11	−2.85	0.52	0.05	−2.68	1.44	2.44
	di-σ	−1.82	−2.56	1.72	0.02	−3.56	1.52	2.85
10	π	−1.88	−2.62	0.45	0.15	−2.48	1.43	2.43
	di-σ	−1.77	−2.51	1.71	0.13	−3.61	1.52	2.85

3.4. Adsorption of Ethylene on Al_2O_3(110)-Supported Ir_n

Next, we studied the adsorption of ethylene on hydrated γ-Al_2O_3(110)-supported Ir_n clusters. For ethylene adsorption on Ir_n/γ-Al_2O_3, besides the three scenarios described on the bare Ir_n cluster, one more scenario was considered: the di-σ′ mode at the interface with one carbon atom on the

Ir_n cluster and one carbon atom on the γ-Al_2O_3 support. Therefore, for ethylene adsorption on Ir_n/γ-Al_2O_3, we considered four possible adsorption geometries, including three modes on the supported Ir_n cluster (π, B-T, and di-σ) and one mode at the interface (di-σ'). The most stable configuration for each mode and their corresponding energies are summarized in Figures 4 and 5 and Table 2.

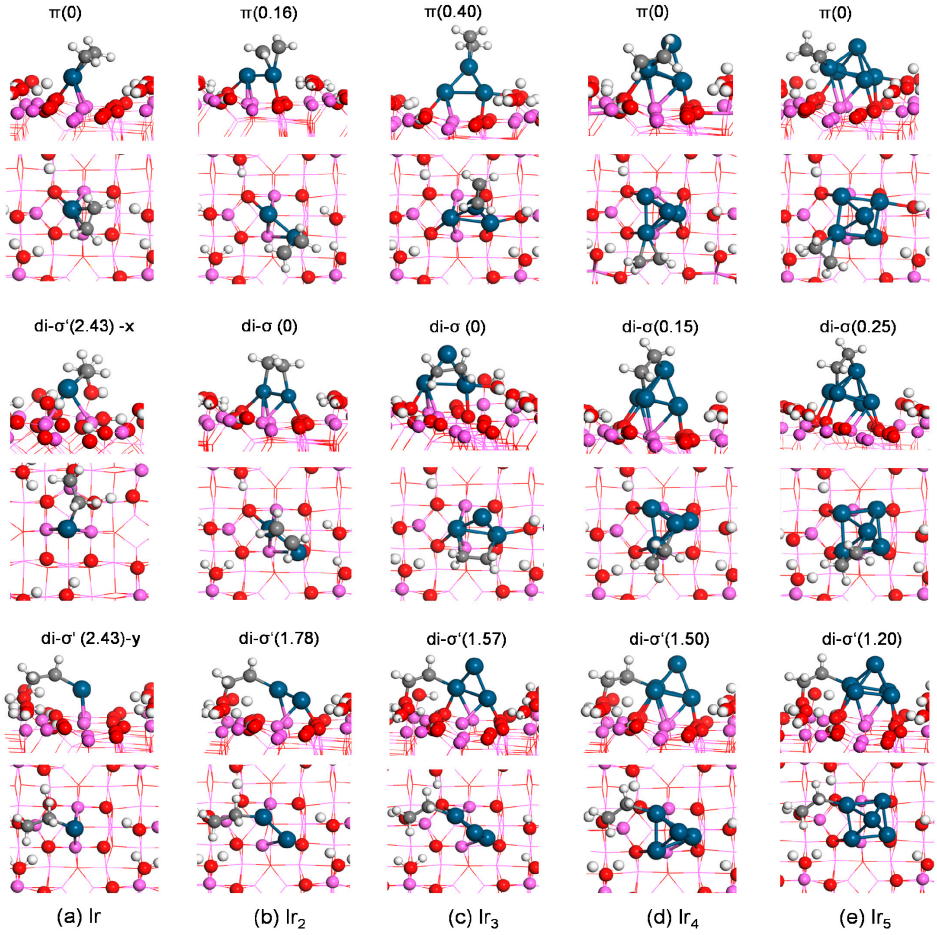

Figure 4. Side view (top) and top view (bottom) of most stable structure for each ethylene-binding mode on γ-Al_2O_3(110)-supported Ir_n (n = 1–5). The energy difference (eV) with respect to the most stable configuration (energy set to 0) is labeled at the top of the structure. For the di-σ' mode at the interface on supported Ir monomer, x and y are the different views of the same structure along two directions. The largest spheres are Ir, and the other color/label scheme is identical to Figure 1.

Ethylene adsorption yielded almost the identical adsorption energy of −2.95 eV both on Ir_1/γ-Al_2O_3(110) and on atomic Ir. The di-σ' mode at the interface, where one carbon atom of ethylene bonds to the Ir atom and the other carbon end bonds to the oxygen site of the surface hydroxyl group, was less stable by 2.42 eV in energy.

For ethylene adsorption on Ir_2/γ-Al_2O_3(110), the di-σ structure was energetically more favorable than the π state (Figure 4b). The adsorption energy of the di-σ mode was −2.26 eV, while the π mode gave E_{ads} of −2.10 eV. As was the case for Ir_1/γ-Al_2O_3(110), the di-σ' structure at the interface resulted in much higher E_{ads} of −0.48 eV, indicating this structure was less favorable than the di-σ and π structures on the supported Ir_2 cluster thermodynamically.

Three π and three di-σ structures were obtained for ethylene adsorption on Ir_3/γ-Al_2O_3(110) through geometry optimization. In the most stable π mode (Figure 4c), ethylene preferred to adsorb on the upper Ir site while in the most favorable di-σ mode, two carbon ends bonded to the bottom Ir centers. The adsorption energies of the di-σ structure and the π mode were −1.99 and −1.75 eV,

respectively, indicating the preference of the di-σ structure. The most stable di-σ′ structure at the interface (of three obtained structures) yielded E_{ads} of −0.58 eV.

Our calculations obtained five di-σ, six π, three monodentate (M) with one carbon end adsorbing on a metal site (Figure S1a), and two di-σ′ structures at the interface for ethylene adsorption on Ir_4/γ-Al_2O_3. The most stable π mode yielded E_{ads} of −1.94 eV. While the most stable di-σ structure yielded E_{ads} of −1.79 eV (Figure 4d). The di-σ′ structure at the interface with one carbon end at a bottom Ir site and one carbon end at the oxygen O(G) site in the hydroxyl group of the γ-Al_2O_3(110) surface yielded E_{ads} of −0.44 eV. The most stable M mode yielded E_{ads} of –0.66 eV. The stability of the ethylene adsorption mode decreased in the order of π > di-σ > M > di-σ′ (at interface).

For ethylene adsorption on Ir_5/γ-Al_2O_3, ethylene binded to one bottom Ir atom resulting in E_{ads} of −1.84 eV in the most stable π mode (of four local equilibrium geometries found). Ethylene adsorbed on the substrate through its two C atoms bonding to one bottom Ir and one upper Ir (di-σ) yielding E_{ads} of −1.59 eV. Two di-σ′ structures at the interface yielded very close E_{ads}, with an energy difference of 0.08 eV (the more stable one is shown in Figure 4e).

On Ir_6/γ-Al_2O_3, the most stable π-bound ethylene yielded E_{ads} of −1.71 eV (Figure 5a). It adsorbed on a bottom Ir atom. The most stable di-σ-bound structure yielded an adsorption energy of −1.54 eV and bridged one top and one bottom Ir atoms. The most stable di-σ′ structure at the interface (of two local equilibrium geometries) on Ir_6/γ-Al_2O_3(110), with one carbon atom on a bottom Ir atom and one carbon atom on the oxygen site of surface hydroxyl, yielded E_{ads} of −0.56 eV.

Although the most stable supported Ir_6 exhibited a triangular-prism configuration and the octahedral structure was less stable by 1.76 eV (higher in energy), as discussed in Section 3.2, the supported octahedral Ir_6 cluster was observed by the experiments. Therefore, the adsorption of ethylene on the most stable supported octahedral Ir_6 cluster was studied for comparison. On Ir_{6oct}/γ-Al_2O_3, the most stable π-bound ethylene yielded E_{ads} of −2.19 eV (Figure 5b). It adsorbed on a top Ir atom with two Ir–C bond lengths both of 2.11 Å. The most stable di-σ-bound structure yielded an adsorption energy of −1.91 eV. It bridged one top Ir atom and one middle Ir atom. The present results agree with the previous experimental observation [9] and theoretical results [34,35]. Qi et al. [34] and Valero et al. [35] discovered that the π adsorption mode was more stable than the di-σ mode for ethylene adsorption on $Ir_{4\text{-}C}/\gamma$-Al_2O_3(110) and Pd_4/γ-Al_2O_3(110) catalyst. Argo et al. [9] observed that the π adsorption mode was directly relevant to the hydrogenation reaction on Ir_n/γ-Al_2O_3 (n = 4 and 6). The most stable M structure (of three local-energy minimum structures, Figure S1b) yielded E_{ads} of −0.62 eV. The di-σ′ (at interface) structure yielded E_{ads} of +0.82 eV suggesting the adsorption was meta-stable and strongly endothermic.

For ethylene adsorption on Ir_7/γ-Al_2O_3, five local equilibrium geometries for both the π and di-σ modes were found. The most stable π state resulted in E_{ads} of −1.96 eV (Figure 5c). The most stable di-σ structure was less stable than the π state, with E_{ads} of −1.79 eV. The di-σ′ structure at the interface yielded E_{ads} of −0.56 eV. Therefore, the stability of these structures decreases in the order π > di-σ > di-σ′ (at interface).

We found three π and four di-σ-bound local-energy minimum structures for ethylene adsorption on Ir_8/γ-Al_2O_3. Analogous to the case on the bare Ir_8 cluster, the di-σ configuration was energetically preferred over the π state by 0.18 eV (lower in energy). For the most stable π and di-σ structures, ethylene preferred to adsorb on the upper Ir atoms away from the interface (Figure 5d). The most stable di-σ′ structure at the interface among two obtained local minima yielded an adsorption energy of −0.25 eV, suggesting less stability than the other two modes.

For ethylene adsorption on Ir_9/γ-Al_2O_3, geometry optimization obtained four π and three di-σ structures. In the most stable π and di-σ structures, ethylene preferred to adsorb on the Ir atom, capping on the face of the cube (Figure 5e). Unlike the case on the bare Ir_9 cluster, the π structure was less stable than the di-σ state. The corresponding adsorption energies E_{ads} were −1.61 and −1.74 eV for the π and di-σ structures, respectively. For ethylene adsorption at the interface, the adsorption was nearly neutral, with E_{ads} of −0.02 eV.

For ethylene adsorption on Ir_{10}/γ-Al_2O_3, the most stable π (of five local minima) and di-σ (of four local equilibrium geometries) structures are provided in Figure 5f. Ethylene adsorbed on the upper Ir atom of the cube in the most stable π mode. In the most stable di-σ mode, ethylene adsorbed on the top surface away from the interface where it bridged one Ir atom of the cube and one caped Ir atom. The most stable π structure yielded an adsorption energy of -1.59 eV, 0.27 eV lower in energy than the most stable di-σ state and suggesting the preference of π structure. Similar to the case on supported Ir_9, ethylene adsorption at the interface of Ir_{10}/γ-Al_2O_3, with one carbon bonding to one surface oxygen atom and the other carbon bonding to one bottom Ir site, was slightly endothermic, with E_{ads} of +0.07 eV.

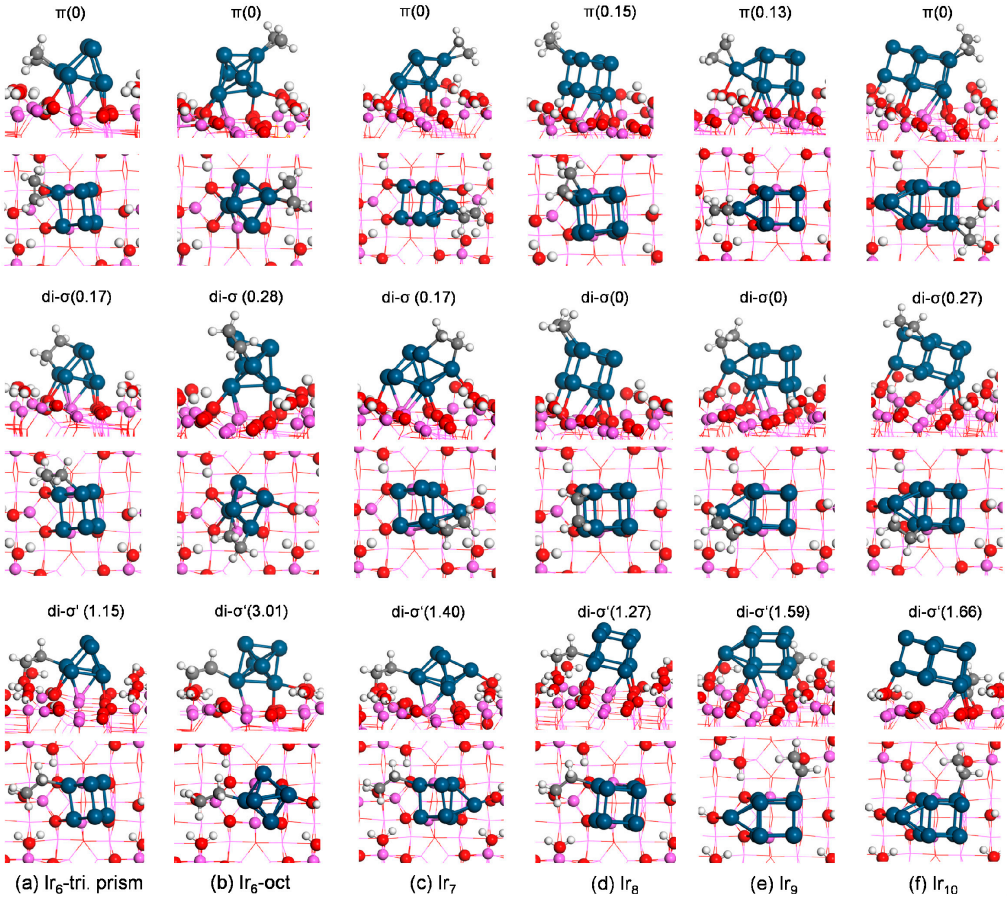

Figure 5. Side (top row) and top views (bottom row) of the most stable structure for each ethylene-binding mode on γ-Al_2O_3(110)-supported Ir_n (n = 6–10). The energy difference (eV) with respect to the most stable configuration (energy set to 0) is labeled at the top of the figure. The color/label scheme is identical to Figure 4.

As shown in Tables 1 and 2, the di-σ mode (either at the interface or on the Ir_n cluster) caused a stronger distortion of the adsorbed ethylene associated with the larger deformation energy $E_{def}(C_2H_4)$ than the π state. This was due to the fundamental nature of the bonds. The bonding in these modes involved a rehybridization of the carbon centers. In Tables 1 and 2, we provide the mean hybridization value according to the work of [35]. According to this work, the mean hybridization value of the gas-phase ethylene—whose carbon center exhibits sp^2 hybridization—was 2, and the carbon center with sp^3 hybridization (e.g., C in ethane) yielded the mean hybridization value of 3. We found the mean hybridization value of the di-σ' mode at the interface was about 3, indicating a complete rehybridization of the carbon centers from sp^2 in the gas phase to sp^3 in the adsorbed state. The di-σ structure at the interface exhibited the same structure with the gas-phase ethane where two H atoms of ethane were substituted by one Ir atom and one surface O (see Figure 3a). The mean

hybridization values of the di-σ and π states on the Ir_n cluster were ~2.45 and ~2.85, indicating a weaker rehybridization of the carbon centers in the π state than the di-σ structures regarding the gas-phase ethylene (the mean hybridization value was 2). These results reveal an electron transfer from the support to π* orbitals of ethylene. A linear relationship between the deformation energy of ethylene and the mean hybridization value of the carbon centers can be observed in Figure S2.

It is noted that Ir_{6oct}/γ-Al_2O_3 exhibited the largest deformation energy upon ethylene adsorption, suggesting the strongest reconstruction among all considered Ir_n/γ-Al_2O_3. Because of the steric hindrance effect, which limits space at the interface, the supported octahedral Ir_6 rearranged itself to accommodate the adsorbed ethylene molecule. Meanwhile the ethylene-support interaction energy was not large enough to balance the deformation energies, resulting in the largest positive E_{ads} of +0.82 eV and indicating the adsorption at the interface was the weakest among all the considered configurations and strongly meta-stable.

Table 2. Adsorption energy E_{ads} (eV), standard adsorption Gibbs free energy at 300 K with the partial pressure of ethylene at 1atm ΔG^{Θ}_{ads}(300 K) (eV), ethylene deformation energy $E_{def}(C_2H_4)$ (eV), substrate deformation energy $E_{def}(Ir_n/\gamma$-$Al_2O_3)$ (eV), interaction energy E_{int} (eV), carbon–carbon bond distance $d_{C\text{-}C}$ (Å), and mean hybridization value (hyd.) for ethylene adsorption on hydrated γ-Al_2O_3(110)-supported Ir_n (n = 1–10) clusters.

n	mode[a]	E_{ads}	ΔG^{Θ}_{ads}(300 K)	$E_{def}(C_2H_4)$	$E_{def}(Ir_n/\gamma$-$Al_2O_3)$	E_{int}	$d_{C\text{-}C}$	hyb.
1	π	−2.95	−3.69	0.61	0.04	−3.60	1.44	2.51
	di-σ′	−0.53	−1.27	3.75	1.49	−5.77	1.52	3.00
2	π	−2.10	−2.84	0.53	0.19	−2.82	1.44	2.45
	di-σ	−2.26	−3.00	1.70	0.73	−4.69	1.51	2.80
	di-σ′	−0.48	−1.22	3.87	1.06	−5.41	1.51	2.98
3	π	−1.75	−2.49	0.55	0.11	−2.41	1.44	2.46
	di-σ	−2.15	−2.89	1.91	0.69	−4.75	1.52	2.93
	di-σ′	−0.58	−1.32	3.73	1.08	−5.39	1.51	2.96
4	π	−1.94	−2.68	0.48	0.32	−2.74	1.42	2.45
	di-σ	−1.79	−2.53	1.55	0.15	−3.49	1.51	2.84
	di-σ′	−0.44	−1.18	3.72	1.08	−5.24	1.48	2.97
5	π	−1.84	−2.58	0.52	0.02	−2.38	1.43	2.48
	di-σ	−1.59	−2.33	1.65	0.08	−3.32	1.51	2.84
	di-σ′	−0.64	−1.38	3.92	0.87	−5.43	1.51	2.96
6tri	π	−1.71	−2.45	0.48	0.20	−2.39	1.42	2.44
	di-σ	−1.54	−2.28	1.71	0.06	−3.31	1.52	2.87
	di-σ′	−0.56	−1.30	3.75	0.99	−5.30	1.51	2.96
6oct	π	−2.19	−2.93	0.58	0.24	−3.01	1.44	2.47
	di-σ	−1.91	−2.65	1.76	0.27	−3.94	1.52	2.86
	di-σ′	+0.82	0.08	3.69	1.58	−4.45	1.51	2.95
7	π	−1.96	−2.70	0.57	0.19	−2.72	1.44	2.48
	di-σ	−1.79	−2.53	1.42	0.48	−3.69	1.49	2.84
	di-σ′	−0.56	−1.30	3.72	0.85	−5.13	1.52	2.99
8	π	−1.52	−2.26	0.55	0.09	−2.16	1.44	2.46
	di-σ	−1.67	−2.41	1.75	0.07	−3.49	1.52	2.85
	di-σ′	−0.25	−0.99	3.68	0.90	−4.83	1.51	2.96
9	π	−1.61	−2.35	0.54	0.19	−2.34	1.43	2.49
	di-σ	−1.74	−2.48	1.49	0.38	−3.61	1.49	2.78
	di-σ′	−0.02	−0.76	3.67	1.09	−4.78	1.51	2.99
10	π	−1.59	−2.33	0.53	0.18	−2.30	1.43	2.48
	di-σ	−1.32	−2.06	1.57	0.13	−3.02	1.50	2.82
	di-σ′	+0.07	−0.67	3.66	1.10	−4.69	1.51	3.00

[1] π and di-σ: two C atoms bond to Ir atom(s); di-σ′: di-σ mode at the interface where one C atom binds to O of the support and the other C atom binds to Ir.

3.5. Thermodynamics

The adsorption Gibbs free energy ΔG_{ads}(T, P) is shown in Figure 6. According to the previous work [36–39], typical molecular adsorption enthalpies for ethylene on silica-supported metal (Pt and Pd) surfaces are about 1.20–1.40 eV in absolute size at 300 K. Our calculation showed that standard

adsorption Gibbs free energy at 300 K, with the partial pressure of ethylene at 1 atm, $\Delta G^{\Theta}_{ads}(300\ K)$ for ethylene adsorption on the Ir(111) surface [33], fell within the same thermodynamic window as $\Delta G^{\Theta}_{ads}(300\ K)$ of 1.32–1.45 eV in absolute size at 1/3 monolayer coverage. Meanwhile, for ethylene adsorption on γ-Al_2O_3-supported Ir_n clusters, the calculated $\Delta G^{\Theta}_{ads}(300\ K)$ for the most stable π and di-σ structures yielded an energy range between −2.07 and −3.70 eV (Figure 6). This suggest that the ethylene–Ir_n interactions were much stronger than the ethylene–Ir(111) interactions. And from the thermodynamic view, ethylene adsorption on the bare and supported Ir_n clusters were much more favorable than those on the Ir(111) surface.

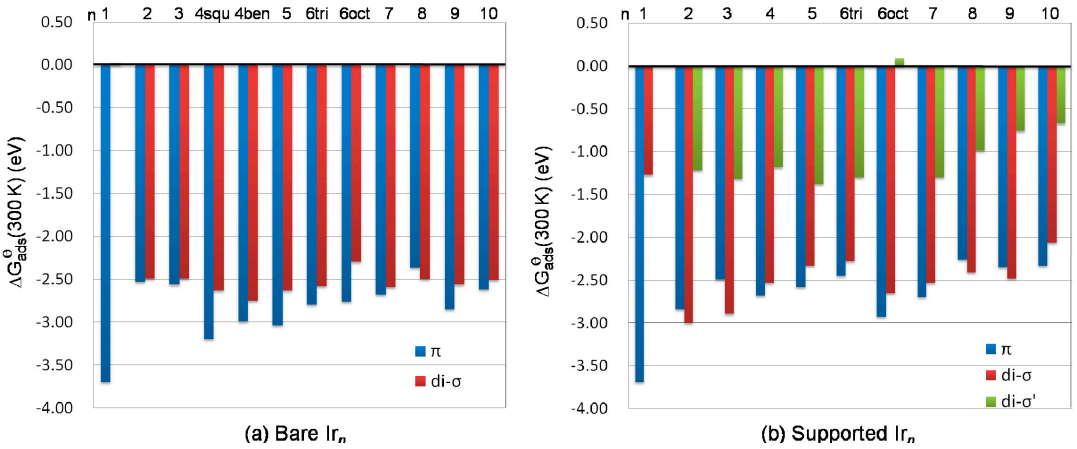

Figure 6. Standard adsorption Gibbs free energy at 300 K; $\Delta G^{q}_{ads}(300\ K)$ of ethylene adsorption on (a) bare Ir_n clusters and (b) hydrated (110) γ-Al_2O_3-supported Ir_n clusters.

The di-σ' structure at the interface gave an energy range between +0.09 and −1.38 eV. Due to the limited space at the interface for the supported octahedral Ir_{6oct} cluster, ethylene adsorption at the interface via di-σ' yielded a positive $\Delta G^{\Theta}_{ads}(300\ K)$ value, indicating ethylene adsorption at the interface at 300 K with partial pressure of ethylene of 1 atm is thermodynamically unfavorable.

3.6. Analysis of Electronic Properties

To know more about the charge redistribution upon the adsorption, we examined the local charge flow for adsorbed monomer, Ir_4, and Ir_{10} systems using electron density difference maps. The electron density difference ($\Delta\rho$) was calculated by

$$\Delta\rho = \rho(\text{Ads/Sub}) - \rho(\text{Ads})_{\text{fix}} - \rho(\text{Sub})_{\text{fix}} \quad (6)$$

where ρ(Ads/Sub) is the total electron density of the adsorbates/substrate complex, $\rho(\text{Ads})_{\text{fix}}$, and $\rho(\text{Sub})_{\text{fix}}$ are the electron densities of the isolated adsorbates and substrate in the same geometry as the adsorbed state, respectively.

In the electron density difference maps (Figure 7), some *d* orbitals of Ir were depleted upon Ir_n cluster adsorption on the surface, which was associated with the charge redistribution of the formed Ir–O and Ir–Al bonds. Oxygen atoms, which bond to Ir atoms, lose electrons during the adsorption process, causing decreased electron density along the Ir–O bond, while in the regions of the Ir–Al bond, electron density increases. Similar phenomena have been observed for Pd [40] and Rh [25] cluster adsorption on γ-Al_2O_3. The depletion of Rh (Pd) *d* orbitals during its adsorption on γ-Al_2O_3 was balanced by increased electron density along the Rh(Pd)–Al bond.

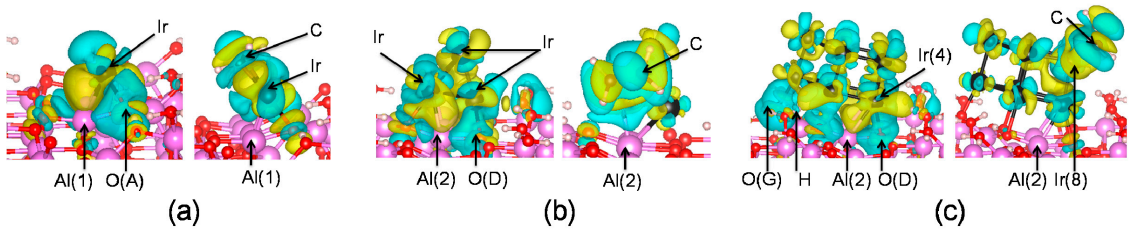

Figure 7. Electron density difference map for hydrated γ-Al_2O_3(110)-supported (**a**) Ir atom, (**b**) Ir_4, and (**c**) Ir_{10} systems. Left column: Ir_n cluster adsorbed on γ-Al_2O_3; right column: ethylene adsorbed on Ir_n/γ-Al_2O_3. Depletion regions: blue; accumulation region: yellow.

As shown in Figure 7, electrons previously accumulated along Ir–Al bonds in Ir_n/γ-Al_2O_3 were transferred to the Ir_n/C_2H_4 part upon C_2H_4 adsorption on γ-Al_2O_3-supported Ir_n. This suggests that the adsorption of ethylene on γ-Al_2O_3-supported Ir_n influences the charge distribution at the metal–alumina interface. The following projected density of states (PDOS) analysis further confirms this statement.

The PDOS are summarized in Figure 8 for the Ir_1/γ-Al_2O_3 and Ir_{10}/γ-Al_2O_3 systems before and after ethylene adsorption. O(A)-Ir(1) and O(D)-Ir(4) were chosen to analyze the metal–support interaction for Ir_1/γ-Al_2O_3 and Ir_{10}/γ-Al_2O_3, respectively.

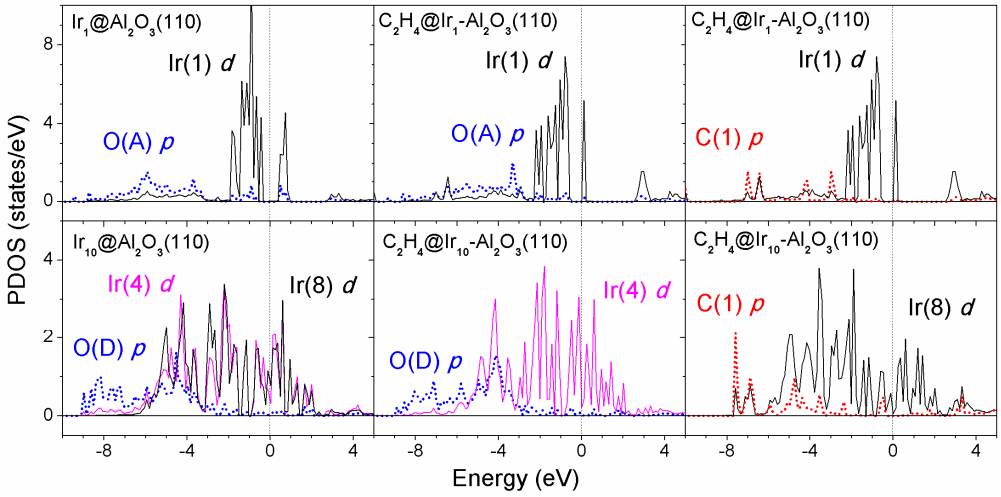

Figure 8. Density of states for the supported Ir_1 (upper row) and Ir_{10} (bottom row) clusters on the hydrated γ-Al_2O_3 (110) surface projected on the bonded Ir atom, surface O, and C in the adsorbed ethylene (π mode) before and after ethylene adsorption. (Dotted lines: p states; solid lines: d states.).

Before ethylene adsorption, the *d* band states of Ir monomer on the alumina support were quite localized and showed an energy gap of ~0.8 eV, while for the supported Ir_{10} cluster, broad and delocalized *d* states (either Ir(4) or Ir(8) atoms) showed up and exhibited a finite density of states at the Fermi level. After ethylene adsorption, the *d* band states became a little smoother for the supported Ir monomer but still localized at the metal cluster, while for the supported Ir_{10} cluster the *d* band states became sharper upon ethylene adsorption. We note that the Ir atom in contact with the support but away from the adsorbed ethylene—Ir(4) as labeled—yielded sharper *d* band states after ethylene adsorption compared with the case before ethylene adsorption. This means the adsorbed ethylene induced charge redistribution at the iridium–alumina interface. The *p* orbitals of oxygen (carbon) atoms strongly mixed with the low-energy (typically below -3 eV) *d* states of Ir atoms.

3.7. Effect of Adsorbed Ethylene on Nucleation of Ir_n Clusters on γ-Al_2O_3

We notice that the di-σ′ adsorption mode at the interface of $Ir_n(n = 1–8)/\gamma$-Al_2O_3 occurred at the same place. This raises the question of whether the pre-adsorbed ethylene at the interface would have affected the growth of Ir_n clusters on the support. To answer this question, we calculated the nucleation energy according to the following equations.

The nucleation or growth energy of Ir_n clusters from a combination of an adsorbed monomer and an Ir_{n-1} was defined by

$$E_{nuc} = E(Ir_n/\gamma\text{-}Al_2O_3) + E(\gamma\text{-}Al_2O_3) - E(Ir_{n-1}/\gamma\text{-}Al_2O_3) - E(Ir_1/\gamma\text{-}Al_2O_3) \quad (7)$$

For pre-adsorbed ethylene at the interface (di-σ′ mode) of Ir_n/γ-Al_2O_3, the nucleation energy E_{nuc} was obtained by

$$E_{nuc} = E(C_2H_4\text{-}Ir_n/\gamma\text{-}Al_2O_3) + E(\gamma\text{-}Al_2O_3) - E(C_2H_4\text{-}Ir_{n-1}/\gamma\text{-}Al_2O_3) - E(Ir_1/\gamma\text{-}Al_2O_3) \quad (8)$$

For the nucleation of the gas-phase Ir_n clusters, the nucleation energy E_{nuc} was calculated using

$$E_{nuc} = E(Ir_n) - E(Ir_{n-1}) - E(Ir_1) \quad (9)$$

For pre-adsorbed ethylene on the gas-phase Ir_n clusters, the nucleation energy was defined by

$$E_{nuc} = E(C_2H_4/Ir_n) - E(C_2H_4\text{-}Ir_{n-1}) - E(Ir_1) \quad (10)$$

Only the most favorable structure is considered for each cluster size.

As shown in Figure 9, the nucleation energies for all Ir cluster sizes we considered were negative, indicating the critical cluster size for Ir growth is 2. Each nucleation step was exothermic, indicating the nucleation process is thermodynamically favorable. In other words, Ir atoms prefer to grow into nanosize Ir_n clusters atom by atom both in the gas phase and on the γ-Al_2O_3 surface, which is consistent with the experimental observation. Yentekakis et al. [41] observed the Ir particle agglomeration on γ-Al_2O_3 in the methane dry reformation reaction using transmission electron microscopy.

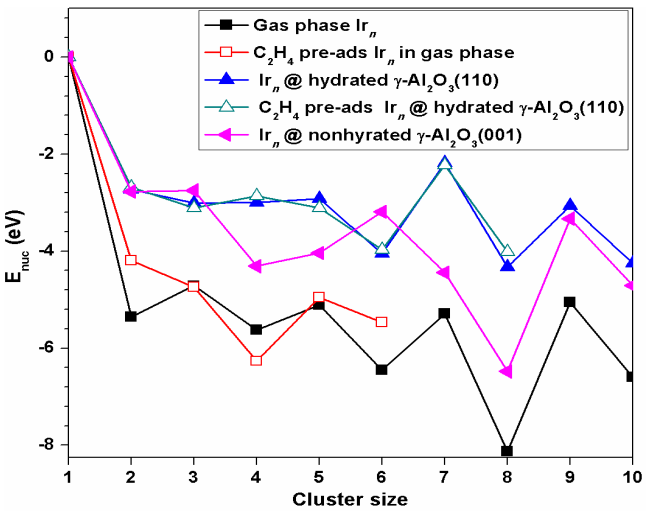

Figure 9. Nucleation energies E_{nuc} of the gas-phase Ir_n cluster; ethylene pre-adsorbed Ir_n in the phase via the π mode; Ir_n on hydrated γ-Al_2O_3(110); and ethylene pre-adsorbed at the interface of Ir_n/γ-Al_2O_3 (110). For comparison, nucleation energy for Ir_n on γ-Al_2O_3(001) [13] is also included.

An E_{nuc} comparison between hydrated (110) and non-hydrated (001) γ-Al_2O_3 surfaces revealed that except for Ir_3 and Ir_6 clusters, the nucleation of Ir_n clusters were less favorable on the hydrated

γ-Al_2O_3 (110) than the non-hydrated γ-Al_2O_3 (001). For Ir_3 and Ir_6 clusters, the trend was reversed. The corresponding E_{nuc} for Ir_3 and Ir_6 on the hydrated (110) surface was 0.26 and 0.86 eV lower than those on the non-hydrated (001) surface, respectively. It should be pointed out that Ir_6 exhibited different adsorption configurations on two surfaces. Chen et al. [13] found the most stable Ir_6 adsorption configuration was an octahedron structure on the non-hydrated γ-Al_2O_3(001) surface, while on the hydrated γ-Al_2O_3(110) we found the octahedron structure of Ir_6 was less stable by 1.76 eV (higher in energy) than the triangular prism (which was the most stable in the gas phase also).

A comparison of the nucleation energies of Ir_n on the hydrated γ-Al_2O_3(110) and pre-adsorbed ethylene at the interface (di-σ' mode) of Ir_n/γ-Al_2O_3(110) suggests that the pre-adsorbed ethylene facilitated the nucleation from the even-sized supported Ir_n to the odd-sized Ir_n clusters, but hindered the nucleation from the odd-sized Ir_n to the even-sized Ir_n clusters. For ethylene pre-adsorbed Ir_n in the gas phase via the π mode, the pre-adsorbed ethylene hindered the nucleation of Ir_n (n = 2, 5, and 6), facilitated the nucleation of Ir_4 from the Ir_3 cluster, and had no effect on the nucleation of Ir_3 from Ir_2.

4. Conclusions

Understanding the adsorption properties of ethylene on supported metal clusters at the atomic level is of great significance for the design of nanocatalysts and their applications in fine chemistry and petroleum refining. The interaction of ethylene with the bare and hydrated γ-Al_2O_3 (110)-supported Ir_n (n = 1–10) clusters was systematically studied by DFT calculations using periodic models. We first identified the most favorable configurations of Ir_n (n = 1–10) clusters on the γ-alumina support. For Ir_n (n = 1–6 and 8) with a cluster diameter smaller than 4.11 Å, the Ir_n cluster adsorbed on the surface O and Al sites only, while for Ir_n (n = 7, 9, and 10) with a cluster diameter larger than 4.21 Å, besides binding to the surface O and Al atoms, the Ir_n cluster binded to the oxygen of surface hydroxyl as well. The γ–Al_2O_3 (110) support changed the morphological features and the cluster stability of Ir_3 and Ir_4 upon their adsorption on the support.

The stability of ethylene adsorption on the bare Ir_n clusters decreased in the sequence of π > di-σ > B-T, with an exception of Ir_8 where a preference of the di-σ structure over the π structure was found. Compared to ethylene adsorption on the bare Ir_n clusters, the γ-Al_2O_3 support reversed the stability of π and di-σ modes on the supported Ir_n (n = 2, 3, and 9) but kept the same for the other bare and supported Ir_n (n = 4–8 and 10) clusters. For supported Ir_n (n = 2, 3, 8, and 9), the stability of the ethylene adsorption mode decreased in the order di-σ > π > di-σ' (at interface) while, on the supported Ir_n (n = 4–7 and 10), the sequence changed to π > di-σ > M > di-σ' (at interface). M mode was only available on the supported Ir_4 and Ir_{6oct} clusters. The carbon centers of the adsorbed ethylene completely rehybridized at the interface from sp^2 in the gas phase to sp^3 in the adsorbed state, while for adsorptions on Ir_n, the orbital hybridization of the carbon centers in adsorbed ethylene was between sp^2 and sp^3.

Among 21 pairs (for example, the π mode on the bare Ir_1 and supported Ir_1 clusters counts as 1 pair), 6 ethylene adsorption modes on the supported Ir_n clusters were stronger than on the bare ones, including π and di-σ on Ir_2, di-σ mode on Ir_3, π and di-σ on Ir_{6oct}, and π mode on Ir_7. One pair—π mode on the supported and bare Ir_1—showed similar stability. For the remaining 14 pairs, ethylene adsorption on the supported Ir_n clusters was weaker than on the bare ones.

Thermodynamic analysis showed that ethylene adsorption on the bare and supported Ir_n clusters was much more favorable than on the Ir(111) surface. The interface between the Ir_n clusters and γ-Al_2O_3 support provided a new adsorption mode di-σ' (at interface), which was the weakest among all adsorption modes.

The pre-adsorbed ethylene at the interface was found to facilitate the nucleation from the even-sized supported Ir_n to odd-sized Ir_n clusters, but hindered the nucleation from the odd-sized Ir_n to even-sized Ir_n clusters.

The electronic analysis shows that the adsorbed ethylene induced charge redistribution between the support and metal clusters. The *d* band states became a little smoother for the supported Ir

monomer, but still localized to the metal cluster upon ethylene adsorption, while for the supported Ir_{10} cluster, the *d* band states became sharper after ethylene adsorption.

Supplementary Materials: The following are available online at http://www.mdpi.com/2079-4991/9/3/331/s1, Figure S1: M configuration of ethylene adsorption. Figure S2: Linear fitting of ethylene deformation energy $E_{def}(C_2H_4)$ (eV) and mean hybridization value of the carbon center in adsorbed ethylene. Table S1: Geometry, magnetic moment (*M*), and energy of gas phase Ir_n (n = 2–10) Table S2: Adsorption energy E_{ads} (eV) and Nucleation energy E_{nuc} (eV) for Ir_n clusters on γ-Al_2O_3 surfaces.

Author Contributions: DFT simulations, X.-R.S.; data analysis, S.Z., Y.Z., W.G., P.M., N.L., and X.-R.S.; writing—original draft preparation, X.-R.S.; writing—review and editing, W.G., N.L., P.M., and X.-R.S.; supervision, X.-R.S.

Funding: This research was funded by the National Natural Science Foundation of China, grant number 21703137, and the Shanghai Pujiang Program, grant number 17PJ1403100.

Conflicts of Interest: The authors declare no conflict of interest.

References

1. Henry, R.; Komurcu, M.; Ganjkhanlou, Y.; Brogaard, R.Y.; Lu, L.; Jens, K.-J.; Berlier, G.; Olsbye, U. Ethene oligomerization on nickel microporous and mesoporous-supported catalysts: Investigation of the active sites. *Catal. Today* **2018**, *299*, 154–163. [CrossRef]
2. Quesada, J.; Arreola-Sánchez, R.; Faba, L.; Díaz, E.; Rentería-Tapia, V.M.; Ordóñez, S. Effect of Au nanoparticles on the activity of TiO_2 for ethanol upgrading reactions. *Appl. Catal. A Gen.* **2018**, *551*, 23–33. [CrossRef]
3. Keppeler, M.; Bräuning, G.; Radhakrishnan, S.G.; Liu, X.; Jensen, C.; Roduner, E. Reactivity of diatomics and of ethylene on zeolite-supported 13-atom platinum nanoclusters. *Catal. Sci. Technol.* **2016**, *6*, 6814–6823. [CrossRef]
4. Guo, Z.; Liu, Y.; Liu, Y.; Chu, W. Promising SiC support for Pd catalyst in selective hydrogenation of acetylene to ethylene. *Appl. Surf. Sci.* **2018**, *442*, 736–741. [CrossRef]
5. Aho, A.; Eränen, K.; Lemus-Yegres, L.J.; Voss, B.; Gabrielsson, A.; Salmi, T.; Murzin, D.Y. Ethylene epoxidation over supported silver catalysts—Influence of catalyst pretreatment on conversion and selectivity. *J. Chem. Technol. Biotechnol.* **2018**, *93*, 1549–1557. [CrossRef]
6. Sikora, P.; Augustyniak, A.; Cendrowski, K.; Nawrotek, P.; Mijowska, E.; Sikora, P.; Augustyniak, A.; Cendrowski, K.; Nawrotek, P.; Mijowska, E. Antimicrobial Activity of Al_2O_3, CuO, Fe_3O_4, and ZnO Nanoparticles in Scope of Their Further Application in Cement-Based Building Materials. *Nanomaterials* **2018**, *8*, 212. [CrossRef] [PubMed]
7. Bruk, L.; Titov, D.; Ustyugov, A.; Zubavichus, Y.; Chernikova, V.; Tkachenko, O.; Kustov, L.; Murzin, V.; Oshanina, I.; Temkin, O. The Mechanism of Low-Temperature Oxidation of Carbon Monoxide by Oxygen over the $PdCl_2$–$CuCl_2$/γ-Al_2O_3 Nanocatalyst. *Nanomaterials* **2018**, *8*, 217. [CrossRef] [PubMed]
8. D'Ippolito, S.A.; Ballarini, A.D.; Pieck, C.L. Influence of Support Acidity and Ir Content on the Selective Ring Opening of Decalin over Ir/SiO_2–Al_2O_3. *Energy Fuels* **2017**, *31*, 5461–5471. [CrossRef]
9. Argo, A.M.; Odzak, J.F.; Gates, B.C. Role of cluster size in catalysis: Spectroscopic investigation of gamma-Al_2O_3-supported Ir_4 and Ir_6 during ethene hydrogenation. *J. Am. Chem. Soc.* **2003**, *125*, 7107–7115. [CrossRef] [PubMed]
10. Argo, A.M.; Odzak, J.F.; Goellner, J.F.; Lai, F.S.; Xiao, F.S.; Gates, B.C. Catalysis by oxide-supported clusters of iridium and rhodium: Hydrogenation of ethene, propene, and toluene. *J. Phys. Chem. B* **2006**, *110*, 1775–1786. [CrossRef] [PubMed]
11. Wang, J.; Yu, H.; Geng, L.; Liu, J.; Han, L.; Chang, L.; Feng, G.; Ling, L. DFT study of Hg adsorption on M-substituted Pd(111) and PdM/γ-Al_2O_3(110) (M = Au, Ag, Cu) surfaces. *Appl. Surf. Sci.* **2015**, *355*, 902–911. [CrossRef]
12. Wang, Y.; Su, Y.; Kang, L. Stability and nucleation of Ir_n (n = 1–5) clusters on different γ-Al_2O_3 surfaces: A density functional theory study. *Phys. Lett. A* **2016**, *380*, 718–725. [CrossRef]
13. Chen, Y.; Huo, M.; Chen, T.; Li, Q.; Sun, Z.; Song, L. The properties of Ir_n (n = 2–10) clusters and their nucleation on γ-Al_2O_3 and MgO surfaces: From ab initio studies. *Phys. Chem. Chem. Phys.* **2015**, *17*, 1680–1687. [CrossRef] [PubMed]

14. Heemeier, M.; Frank, M.; Libuda, J.; Wolter, K.; Kuhlenbeck, H.; Bäumer, M.; Freund, H.J. The influence of OH groups on the growth of rhodium on alumina: A model study. *Catal. Lett.* **2000**, *68*, 19–24. [CrossRef]
15. Libuda, J.; Frank, M.; Sandell, A.; Andersson, S.; Brühwiler, P.A.; Bäumer, M.; Mårtensson, N.; Freund, H.J. Interaction of rhodium with hydroxylated alumina model substrates. *Surf. Sci.* **1997**, *384*, 106–119. [CrossRef]
16. Digne, M.; Sautet, P.; Raybaud, P.; Euzen, P.; Toulhoat, H. Use of DFT to achieve a rational understanding of acid-basic properties of γ-alumina surfaces. *J. Catal.* **2004**, *226*, 54–68. [CrossRef]
17. Digne, M.; Sautet, P.; Raybaud, P.; Euzen, P.; Toulhoat, H. Hydroxyl Groups on γ-Alumina Surfaces: A DFT Study. *J. Catal.* **2002**, *211*, 1–5. [CrossRef]
18. Kresse, G.; Furthmüller, J. Efficiency of ab-initio total energy calculations for metals and semiconductors using a plane-wave basis set. *Comput. Mater. Sci.* **1996**, *6*, 15–50. [CrossRef]
19. Kresse, G.; Furthmüller, J. Efficient iterative schemes for ab-initio total-energy calculations using a plane-wave basis set. *Phys. Rev. B* **1996**, *54*, 11169–11186. [CrossRef]
20. Perdew, J.P.; Chevary, J.A.; Vosko, S.H.; Jackson, K.A.; Pederson, M.R.; Singh, D.J.; Fiolhais, C. Atoms, molecules, solids, and surfaces: Applications of the generalized gradient approximation for exchange and correlation. *Phys. Rev. B* **1992**, *46*, 6671–6687. [CrossRef]
21. Perdew, J.P.; Wang, Y. Accurate and simple analytic representation of the electron-gas correlation energy. *Phys. Rev. B* **1992**, *45*, 13244–13249. [CrossRef]
22. Kresse, G.; Joubert, D. From ultrasoft pseudopotentials to the projector augmented-wave method. *Phys. Rev. B Condens. Matter Mater. Phys.* **1999**, *59*, 1758–1775. [CrossRef]
23. Shi, X.-R.; Wang, S.-G.; Wang, J. Chemisorption of oxygen and subsequent reactions on low index surfaces of β–Mo_2C: Insights from first-principles thermodynamics and kinetics. *J. Mol. Catal. A Chem.* **2016**, *417*, 53–63. [CrossRef]
24. Fulton, J.L.; Linehan, J.C.; Autrey, T.; Balasubramanian, M.; Chen, Y.; Szymczak, N.K. When is a Nanoparticle a Cluster? An Operando EXAFS Study of Amine Borane Dehydrocoupling by $Rh_{4–6}$ Clusters. *J. Am. Chem. Soc.* **2007**, *129*, 11936–11949. [CrossRef] [PubMed]
25. Shi, X.-R.; Sholl, D.S. Nucleation of Rh_n (n = 1–5) Clusters on γ-Al_2O_3 Surfaces: A Density Functional Theory Study. *J. Phys. Chem. C* **2012**, *116*, 10623–10631. [CrossRef]
26. Nigam, S.; Majumder, C. Adsorption of Small Palladium Clusters on the alfa-Al_2O_3(0001) Surface: A First Principles. *Stud. J. Phys. Chem. C* **2012**, *116*, 2863–2871. [CrossRef]
27. Kulkarni, A.; Lobo-Lapidus, R.J.; Gates, B.C. Metal clusters on supports: Synthesis, structure, reactivity, and *catalytic* properties. *Chem. Commun.* **2010**, *46*, 5997–6015. [CrossRef] [PubMed]
28. Du, J.; Sun, X.; Chen, J.; Jiang, G. A theoretical study on small iridium clusters: Structural evolution, electronic and magnetic properties, and reactivity predictors. *J. Phys. Chem. A* **2010**, *114*, 12825–12833. [CrossRef] [PubMed]
29. Pawluk, T.; Hirata, Y.; Wang, L. Studies of iridium nanoparticles using density functional theory calculations. *J. Phys. Chem. B* **2005**, *109*, 20817–20823. [CrossRef] [PubMed]
30. Ravenelle, R.M.; Copeland, J.R.; Kim, W.-G.; Crittenden, J.C.; Sievers, C. Structural Changes of γ-Al_2O_3-Supported Catalysts in Hot Liquid Water. *ACS Catal.* **2011**, *1*, 552–561. [CrossRef]
31. Neurock, M.; van Santen, R.A. A First Principles Analysis of C−H Bond Formation in Ethylene Hydrogenation. *J. Phys. Chem. B* **2000**, *104*, 11127–11145. [CrossRef]
32. Heard, C.J.; Siahrostami, S.; Grönbeck, H. Structural and Energetic Trends of Ethylene Hydrogenation over Transition Metal Surfaces. *J. Phys. Chem. C* **2016**, *120*, 995–1003. [CrossRef]
33. Shi, X.R.; Kong, H.; Wang, S.; Wang, H.; Qin, Z.; Wang, J. Mechanistic Insights into Ethylene Transformations on Ir(111) by Density Functional Calculations and Microkinetic Modeling. *ChemPhysChem* **2017**, *18*, 906–916. [CrossRef] [PubMed]
34. Qi, K.; Zhao, J.-M.; Wang, G.-C. A density functional theory study of ethylene hydrogenation on MgO- and γ-Al_2O_3-supported carbon-containing Ir_4 clusters. *Phys. Chem. Chem. Phys.* **2015**, *17*, 4899–4908. [CrossRef] [PubMed]
35. Valero, M.C.; Raybaud, P.; Sautet, P. Interplay between molecular adsorption and metal-support interaction for small supported metal clusters: CO and C_2H_4 adsorption on Pd_4/gamma-Al_2O_3. *J. Catal.* **2007**, *247*, 339–355. [CrossRef]
36. Natal-Santiago, M.A.; Podkolzin, S.G.; Cortright, R.D.; Dumesic, J.A. Microcalorimetric studies of interactions of ethene, isobutene, and isobutane with silica-supported Pd, Pt, and PtSn. *Catal. Lett.* **1997**, *45*, 155–163. [CrossRef]

37. Shen, J.; Hill, J.M.; Watwe, R.M.; Spiewak, B.E.; Dumesic, J.A. Microcalorimetric, Infrared Spectroscopic, and DFT Studies of Ethylene Adsorption on Pt/SiO_2 and $Pt-Sn/SiO_2$ Catalysts. *J. Phys. Chem. B* **1999**, *103*, 3923–3934. [CrossRef]
38. Shen, J.; Hill, J.M.; Watwe, R.M.; Podkolzin, S.G.; Dumesic, J.A. Ethylene adsorption on $Pt/Au/SiO_2$ catalysts. *Catal. Lett.* **1999**, *60*, 1–9. [CrossRef]
39. Podkolzin, S.G.; Alcala, R.; de Pablo, J.J.; Dumesic, J.A. Monte Carlo Simulations of Reaction Kinetics for Ethane Hydrogenolysis over Pt. *J. Phys. Chem. B* **2002**, *106*, 9604–9612. [CrossRef]
40. Valero, M.C.; Raybaud, P.; Sautet, P. Nucleation of Pd_n (n = 1–5) clusters and wetting of Pd particles on gamma-Al_2O_3 surfaces: A density functional theory study. *Phys. Rev. B* **2007**, *75*, 45427. [CrossRef]
41. Yentekakis, I.V.; Goula, G.; Panagiotopoulou, P.; Katsoni, A.; Diamadopoulos, E.; Mantzavinos, D.; Delimitis, A. Dry Reforming of Methane: Catalytic Performance and Stability of Ir Catalysts Supported on γ-Al_2O_3, $Zr_{0.92}Y_{0.08}O_{2-\delta}$ (YSZ) or $Ce_{0.9}Gd_{0.1}O_{2-\delta}$(GDC) Supports. *Top. Catal.* **2015**, *58*, 1228–1241. [CrossRef]